ISBN: 978-3-95450-253-0 ISSN: 2673-5571 doi:10.18429/JACoW-HB2023-WEA2I2

SPACE CHARGE INDUCED RESONANCES AND SUPPRESSION IN J-PARC MR

T. Yasui*
J-PARC center, KEK&JAEA, Tokai, Naka, Ibaraki, Japan

Abstract

In the main ring synchrotron (MR) of Japan Proton Accelerator Research Complex (J-PARC), we identified that the space charge induced resonance $8\nu_y = 171$ is the main source of beam losses in the neutrino operation, except for random resonances. We found that this resonance can be suppressed by beam optics modification while maintaining the tune. We confirmed the superiority of the newly-developed optics via analytical calculations of resonance potentials, beam loss simulations, Poincaré maps, beam loss measurements, and frequency map analyses.

INTRODUCTION

The main ring synchrotron (MR) [1] of Japan Proton Accelerator Research Complex (J-PARC) is the synchrotron providing high power proton beams to the neutrino and hadron experiments. Eight-bunch beams are injected with a kinetic energy of 3 GeV, and they are accelerated to 30 GeV. In 2021, we operated with an intensity of 2.66×10^{14} protons per pulse (ppp), corresponding to 3.3×10^{13} protons per bunch (ppb), and a cycle time of 2.48 s in the neutrino fast extraction (FX) operation. For further intensity increase, we launched a plan to upgrade the beam power to 1.3 MW in the FX operation [2]. In JFY2022, we made a long-term shutdown for hardware upgrade to realize faster cycling. As a result, the cycle time became 1.36 s. Although the beam intensity was temporarily reduced due to the capability of the RF system, the beam power was recorded at 766 kW [3]. To realize 1.3 MW operation, we are going to increase the beam intensity to 3.3×10^{14} ppp and further reduce the cycle time.

To increase the beam intensity, we need not only to upgrade the RF system but also to control the beam loss. Tracking simulations show that the beam loss occurs even when we assume perfect magnetic fields and alignments because of space-charge-induced resonances. In fact, the beam loss can be found before and during very early stages of acceleration, showing strong space charge effects. The longitudinal beam size becomes stable after approximately 5 ms from beam injection and the space charge effect becomes stable. In this paper, we focus on the period when the longitudinal beam size is stable.

Figure 1 shows the tune spread after the longitudinal beam size has stabilized. It was obtained by the space charge tracking simulation code SCTR [5, 6], which employs the particle-in-cell algorithm. The working point was optimized at $(\nu_x, \nu_y) = (21.35, 21.43)$ [7, 8]. In fact, Fig. 1 shows that most of the particles can avoid the differential resonance

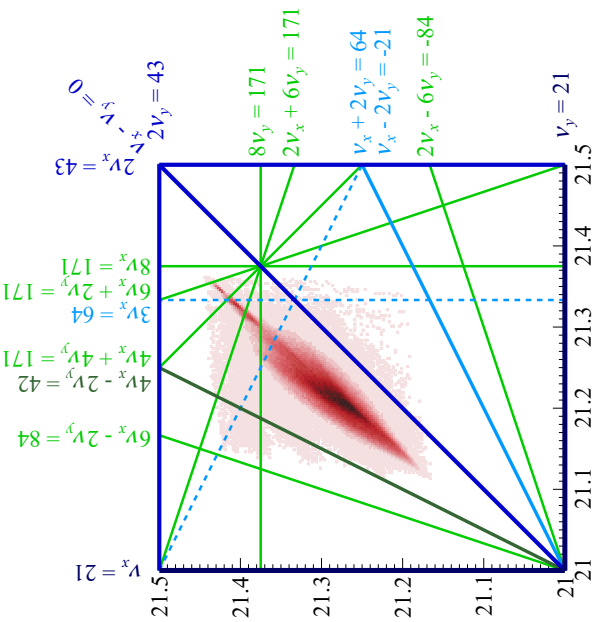

Figure 1: Tune spread (approximately 30 ms from beam injection) and major resonances (lines) in FX operation [4]. The tune spread was obtained by the tracking simulation assuming a beam intensity of 3.2×10^{13} ppb.

$\nu_x - \nu_y = 0$ (or the space-charge-induced 4th-order structure resonance $2\nu_x - 2\nu_y = 0$), the half-integer resonance $2\nu_y = 43$, and the space-charge-induced 6th-order structure resonance $4\nu_x - 2\nu_y = 42$. The beam is crossing the dashed skyblue lines and some of light green lines. The dashed skyblue lines represent the resonances $3\nu_x = 64$ and $\nu_x + 2\nu_y = 64$, which are nonstructure resonances driven by sextupole magnetic fields. They are compensated using four trim coils of sextupole magnets [2]. The light green lines denotes space-charge-induced 8th-order structure resonances. Since the superperiodicity of the MR is only three, it is difficult to completely avoid high-order structure resonances.

IDENTIFICATION OF BEAM LOSS SOURCE

To suppress space charge effects, second harmonic RF cavities are used in the MR. The top panel of Fig. 2 shows the longitudinal phase-space distribution of the beam after stabilization, the middle panel shows its projection to the z coordinate, and the bottom panel shows the distribution of the lost particles. Most of the lost particles are found at locations of high line densities. It shows that the beam loss is caused by space charge effects. It also shows the importance of peak suppression by the second harmonic RF cavities.

* takaaki.yasui@kek.jp

ISBN: 978-3-95450-253-0 ISSN: 2673-5571 doi:10.18429/JACoW-HB2023-WEA2I2

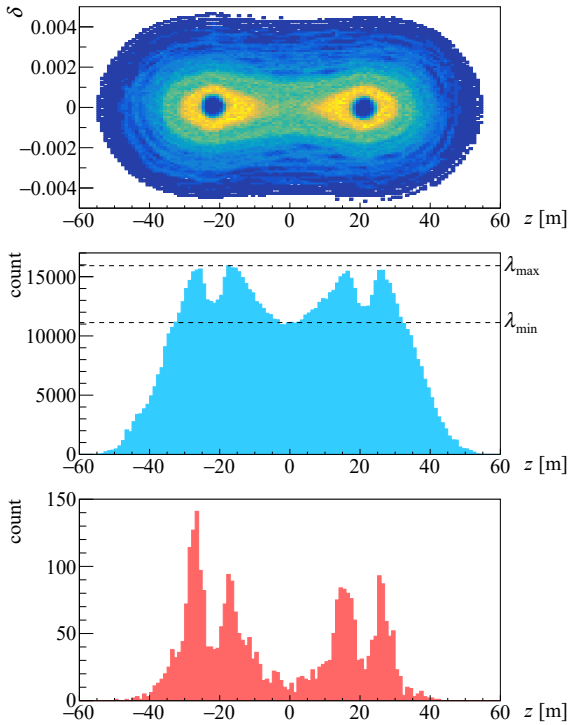

Figure 2: Longitudinal phase-space distribution of the beam (top panel) and its projection to the z coordinate (middle panel), and longitudinal distribution of the lost particles (bottom panel) obtained by SCTR simulations [4].

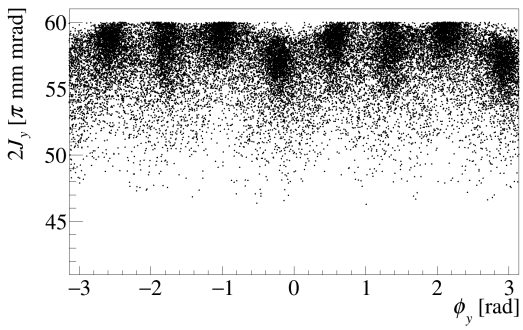

Figure 3: Simulated vertical phase-space distribution of the lost particles which exceeded the vertical aperture $2J_y = 60\,\pi$·mm·mrad [4]. The last 15-turn positions are plotted.

In the MR, the collimators are set so that both horizontal and vertical apertures are approximately $60\,\pi$·mm·mrad. The lost particles are classified as those exceeded the horizontal aperture and those exceeded the vertical aperture. In the SCTR simulation, 71.4 % of the particles were lost because of their high vertical actions. Figure 3 shows the vertical phase-space distribution of the particles which exceeded the vertical aperture $2J_y = 60\,\pi$·mm·mrad. It forms eight islands, indicating the effects of eighth-order vertical resonance $8\nu_y = n$.

Figure 4 shows the tune distribution of the particles which exceeded the vertical aperture $2J_y = 60\,\pi$·mm·mrad. Many particles are lost around the resonance $8\nu_y = 171$ and some are lost around $2\nu_x + 6\nu_y = 171$. It indicates that the primary

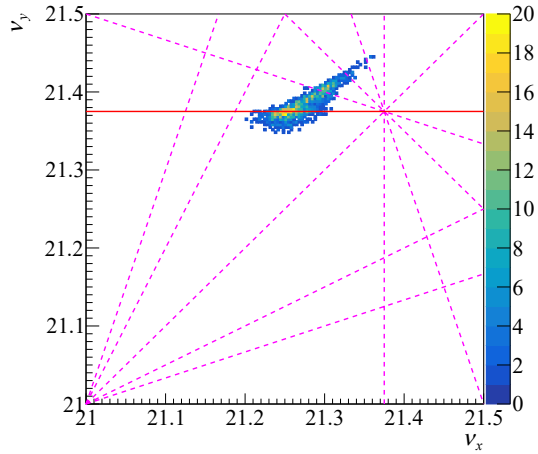

Figure 4: Simulated tune distribution of the lost particles which exceeded the vertical aperture [4]. The red solid line represents the resonance $8\nu_y = 171$, and the magenta dashed lines denote other space charge resonances up to eighth order.

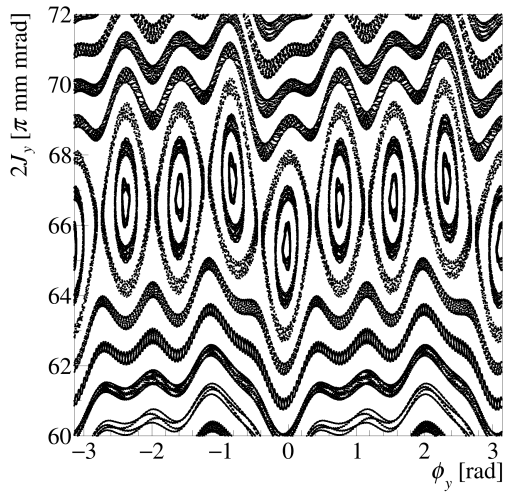

Figure 5: Simulated Poincaré map in the vertical coordinate with the present FX optics [4].

source of the beam loss is the resonance $8\nu_y = 171$ and the secondary source is the resonance $2\nu_x + 6\nu_y = 171$. Both are the eighth-order structure resonances driven by space charge effects.

To confirm the effect of the resonance $8\nu_y = 171$, a vertical Poincaré map was drawn. In this simulation, the space charge effects were calculated using Bassetti-Erskine formula [9], which assumes a two-dimensional Gaussian distribution as the beam distribution. The line density was evaluated from the longitudinal beam distribution (middle panel of Fig. 2). The line density was set to $\lambda = \lambda_{\max} \equiv 4.86 \times 10^{11}$ ppb/m. The initial longitudinal position of the test particles were set to $z = \delta = 0$ and initial horizontal action was set to $J_x = 0$. The result is shown in Fig. 5. Eight resonance islands were clearly observed around $63\pi \lesssim 2J_y \lesssim 69\,\pi$·mm·mrad. It also verifies the effects of the resonance $8\nu_y = 171$.

ISBN: 978-3-95450-253-0 ISSN: 2673-5571 doi:10.18429/JACoW-HB2023-WEA2I2

MECHANISM OF THE BEAM LOSS

In Fig. 1, the working point $(\nu_x, \nu_y) = (21.35, 21.43)$ is in the area surrounded by the resonances $2\nu_y = 43$, $6\nu_x + 2\nu_y = 171$, and $4\nu_x + 4\nu_y = 171$. In this section, we discuss why the resonance $8\nu_y = 171$ was the primary source of the beam loss over the resonances $6\nu_x + 2\nu_y = 171$ and $4\nu_x + 4\nu_y = 171$.

If a low-order strong resonance affects the beam, the beam distribution will be distorted, resulting in beam loss. This phenomenon is often described as beam loss due to emittance growth. In the J-PARC MR, however, we have already avoided such low-order resonances and the transverse rms emittance is stable before the acceleration. In this case, a particle at the center of the six-dimensional beam distribution will not be lost. What can be lost are the particles at the beam halo. In the MR, the beam loss is caused by the resonances which affect particles at beam halo.

To identify the cause of the beam loss, we need to know where resonances affect. A particle is affected by a resonance $m_x\nu_x + m_y\nu_y = n$ when its incoherent tune $\nu_{\text{incoh.}}$ satisfies the on-resonance condition $m_x\nu_{x,\text{incoh.}} + m_y\nu_{y,\text{incoh.}} = n$. The incoherent tune can be written as

$$\nu_{\text{incoh.}} = \nu_{\text{working point}} + \Delta\nu_{\text{space charge}} + \Delta\nu_{\text{sext.}} + \xi\delta, \quad (1)$$

where $\nu_{\text{working point}}$ is the working point, $\Delta\nu_{\text{space charge}}$ is the space charge tune shift, $\Delta\nu_{\text{sext.}}$ is the amplitude dependent tune shift by sextupole magnetic fields and ξ is the chromaticity. The space charge tune shift can be derived from the space charge potential $U_{\text{space charge}}$ by [4]

$$\Delta\nu_{u,\text{space charge}} = \frac{C}{(2\pi)^4}\oint \mathrm{d}\theta \frac{\partial}{\partial J_u}\iint \mathrm{d}\phi_x \mathrm{d}\phi_y U_{\text{space charge}}, \quad (2)$$

where C is the circumference. Assuming a two-dimensional Gaussian distribution, the space charge potential becomes [10]

$$U_{\text{space charge}} = \frac{\lambda r_0}{\gamma_{\text{rel.}}^3\beta_{\text{rel.}}^2}\int_0^\infty \mathrm{d}q \frac{\exp[-\frac{x^2}{2\sigma_x^2+q} - \frac{y^2}{2\sigma_y^2+q}]}{\sqrt{2\sigma_x^2+q}\sqrt{2\sigma_y^2+q}}, \quad (3)$$

where r_0 is the classical radius of the particle, $\gamma_{\text{rel.}}$, $\beta_{\text{rel.}}$ are Lorentz factors and σ_u is the rms beam size. These can be analytically solved as [4, 6, 11]

$$\Delta\nu_{u,\text{space charge}} = -\frac{1}{2\pi}\frac{\lambda r_0}{\gamma_{\text{rel.}}^3\beta_{\text{rel.}}^2}\oint \mathrm{d}s\beta_u \times \int_0^\infty \mathrm{d}q \frac{e^{-w_u-w_v}[I_0(w_u) - I_1(w_u)]I_0(w_v)}{(2\sigma_u^2+q)^{3/2}(2\sigma_v^2+q)^{1/2}}, \quad (4)$$

where β_u is the betatron function, $w_u = J_u\beta_u/(2\sigma_u^2 + q)$ and $I_\nu(z)$ is the modified Bessel function.

In the real beam, the line density is not a constant. With reference to the middle panel of Fig. 2, we set the lower limit $\lambda_{\min} = 3.40 \times 10^{11}$ ppb/m as the line density at $z = 0$.

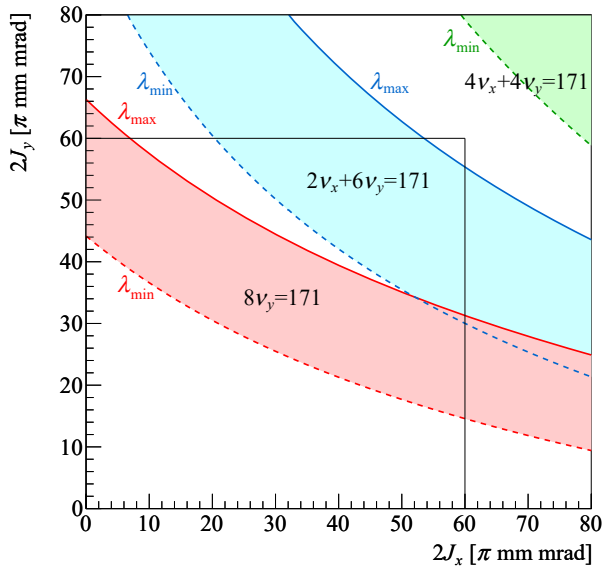

Figure 6: The region of actions where resonances affect [4]. The solid and dashed colored lines represent the actions satisfying on-resonance conditions with $\lambda = \lambda_{\max}, \lambda_{\min}$, respectively. The red, blue, and green lines correspond to the resonances $8\nu_y = 171$, $2\nu_x + 6\nu_y = 171$, and $4\nu_x + 4\nu_y = 171$, respectively. The black lines at $2J_x, 2J_y = 60\,\pi$·mm·mrad represent the apertures.

The region surrounded by $\lambda_{\max}$ and $\lambda_{\min}$, corresponding to $|z| < 33$ m, covers 94.1 % of the beam loss. The line density can be assumed to be in this region.

Figure 6 shows the analytical calculation results of actions satisfying on-resonance conditions for each resonance and the two line densities. In these calculations, we assumed $\delta = 0$. For example, when the line density is $\lambda = \lambda_{\max}$, an on-momentum particle with $2J_x = 0$ and $2J_y = 66.3\,\pi$·mm·mrad has the vertical incoherent tune of $\nu_{y,\text{incoh.}} = 21.375$ and satisfies the on-resonance condition for $8\nu_y = 171$. The region covered by the solutions with $\lambda = \lambda_{\max}, \lambda_{\min}$ can be considered as where the resonance affects. Since the collimator are set to $2J_x = 2J_y = 60\,\pi$·mm·mrad, the beam halo in the J-PARC MR is also $2J_x = 2J_y = 60\,\pi$·mm·mrad. Therefore, the resonances causing the beam loss is the one affecting there. Figure 6 indicates that the resonances $8\nu_y = 171$ and $2\nu_x + 6\nu_y = 171$ affect the beam halo. It shows that these two resonances are the causes of the beam loss and is consistent with the previous conclusion. At $2J_y = 6\,\pi$·mm·mrad, the resonance $8\nu_y = 171$ affects $2J_x \sim 0 - 7\,\pi$·mm·mrad, while the resonance $2\nu_x + 6\nu_y = 171$ affects $2J_x \sim 20\pi - 53\,\pi$·mm·mrad. Considering a Gaussian distribution, the number of the particles affected by the resonance $8\nu_y = 171$ is much larger than those affected by the resonance $2\nu_x + 6\nu_y = 171$. This is why the resonance $8\nu_y = 171$ is the main cause of the beam loss.

ISBN: 978-3-95450-253-0 ISSN: 2673-5571 doi:10.18429/JACoW-HB2023-WEA2I2

NEW BEAM OPTICS FOR REDUCING BEAM LOSS

There are several methods to escape from the effects of resonances. The first method is to change the working point. In the J-PARC MR, however, we have already optimized it around $(\nu_x, \nu_y) = (21.*, 21.*)$ region. If the working point is moved, the beam will hit low-order resonances. The second method is corrector magnets. To correct eighth-order resonances, 16-pole magnets are needed. However, it is costly and technically difficult. The method we used is to consider a new beam optics but maintaining the working point [4].

The space charge potential can be expanded in Fourier series as

$$U = \sum_{m_x,m_y,n} U_{m_x,m_y,n} \cos(m_x\phi_x + m_y\phi_y - n\theta + \xi_{m_x,m_y,n}). \tag{5}$$

In this equation, the Fourier amplitude $U_{m_x,m_y,n}$ characterizes the strength of the resonance $m_x\nu_x + m_y\nu_y = n$. Hereinafter, we define $U_{m_x,m_y,n}$ as the resonance potential. The resonance potential can be derived by Fourier transformation of the potential as

$$U_{m_x,m_y,n}e^{i\xi_{m_x,m_y,n}} = \frac{2}{(2\pi)^3}\oint \mathrm{d}\theta \iint \mathrm{d}\phi_x \mathrm{d}\phi_y U e^{-i[m_x\phi_x + m_y\phi_y + n]}. \tag{6}$$

Assuming a Gaussian distribution, the potential for the resonance $8\nu_y = 171$ can be written as [4]

$$U_{0,8,171}e^{i\xi_{0,8,171}} = \frac{\lambda r_0}{\pi\gamma_{\mathrm{rel.}}^3\beta_{\mathrm{rel.}}^2}\oint \mathrm{d}s e^{i[8\chi_y - (8\nu_y - 171)\theta]} \times \int_0^\infty \mathrm{d}q \frac{e^{-w_x - w_y} I_0(w_x) I_4(w_y)}{\sqrt{2\sigma_x^2 + q}\sqrt{2\sigma_y^2 + q}}, \tag{7}$$

where $\chi_y(s) = \int_0^s \mathrm{d}s/\beta_y$ represents vertical phase advance. Maintaining the working point means that fixing the phase advance in a circumference $\chi_y(C) = 2\pi\nu_y$. Even with this restriction, the phase advance in each place $\chi_y(s)$ is modifiable. In short, $U_{0,8,171}$ is changeable while maintaining the working point.

Even with the restriction of the working point, there are many solutions for the beam optics. As another restriction for the beam optics, we should keep an achromat lattice in the J-PARC MR. In the present optics, the horizontal phase advance in the arc section $\Delta\psi_{x,\mathrm{arc}}$ is set to

$$\Delta\psi_{x,\mathrm{arc}} = 6 \times 2\pi. \tag{8}$$

This relation should be held to maintain the dispersion in the straight section at zero. Another suggestion for the beam optics is to modify it globally rather than locally because the space charge is generated throughout the ring. Considering these conditions, we chose the vertical phase advance in the arc section $\Delta\psi_{y,\mathrm{arc}}$ as a scanning knob. To keep the working point, the vertical phase advance in the straight section $\Delta\psi_{y,\mathrm{straight}}$ was modified at the same time as

$$\Delta\psi_{y,\mathrm{straight}} = (2\pi\nu_y - 3\Delta\psi_{y,\mathrm{arc}})/3, \tag{9}$$

where the term 3 comes from the superperiodicity of the MR.

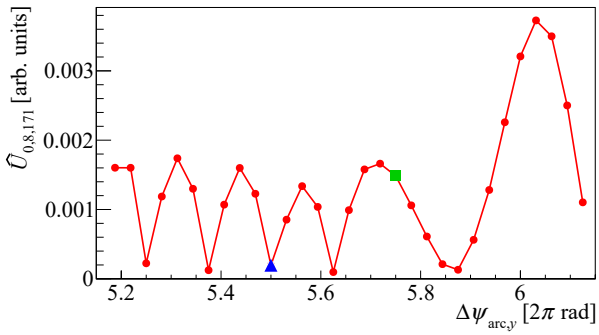

Figure 7: Resonance potentials $U_{0,8,171}$ derived by analytical calculations for each beam optics [4]. The green square and blue triangle denote the results of the present and new optics, respectively.

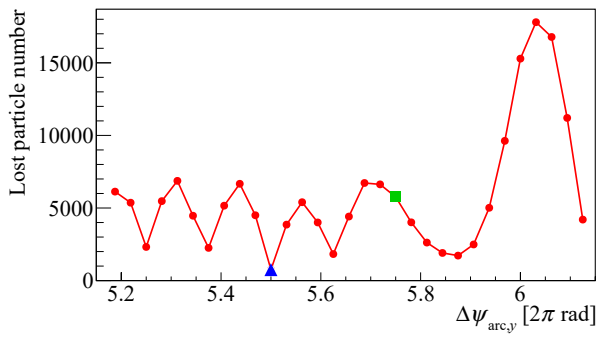

Figure 8: Numbers of the lost particles by tracking simulations for each beam optics [4]. The green square and blue triangle denote the results of the present and new optics, respectively.

Figure 7 shows potentials of the resonance $8\nu_y = 171$ calculated analytically as a function of $\Delta\psi_{y,\mathrm{arc}}$. The present optics is shown as a green square. This result indicates that there are some better beam optics which can weaken the resonance $8\nu_y = 171$. We also simulated the beam loss for all beam optics and the results are shown in Fig. 8. Comparing Figs. 7 and 8, their variations look very similar. It also strongly supports that the beam loss is caused by the resonance $8\nu_y = 171$. To suppress the resonance $8\nu_y = 171$ and reduce the beam loss, we chose the beam optics shown as the blue triangle. Hereinafter, we simply call this optics as the new optics.

Figure 9 shows the vertical Poincaré map with the new optics. The conditions for the simulation were the same as those with the present optics. Although the resonance islands are still visible, their width becomes smaller compared to the present optics. In the present optics, the width of the resonance islands is approximately $6\,\pi$·mm·mrad, while it

ISBN: 978-3-95450-253-0 ISSN: 2673-5571 doi:10.18429/JACoW-HB2023-WEA2I2

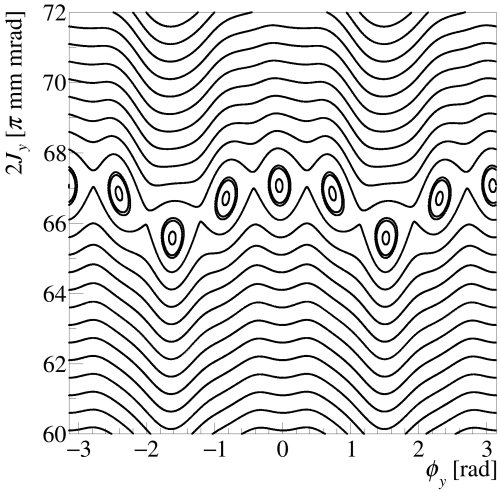

Figure 9: Simulated Poincaré map in the vertical coordinate with the new optics [4].

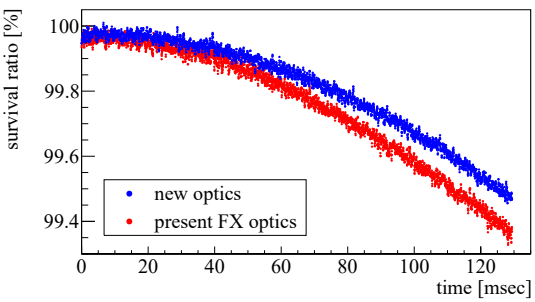

Figure 10: Beam survival ratios measured by the direct-current current transformer (DCCT) with the present (red) and new (blue) optics [4].

is approximately 1.5 π·mm·mrad in the new optics. This clearly shows that the resonance $8\nu_y = 171$ is weakened by applying the new optics.

The beam losses were also measured for both optics. The beam intensity was 3.3×10^{13} ppb and the number of bunches was two. The optics were carefully adjusted and the beta modulations were 3 % for both optics. The sextupole-driven third-order nonstructure resonance $3\nu_x = 64$ and $\nu_x + 2\nu_y = 64$ were simultaneously compensated by trim coils of sextupole magnets for both optics. Figure 10 shows the beam survival ratios measured by the direct-current current transformer (DCCT). By applying the new beam optics, the beam loss was successfully reduced approximately 20 % in 130 ms.

Frequency map analysis (FMA) was also performed to visualize resonances. As the initial beam distribution, the one after 24100 turns of tracking, corresponding to 130 ms, was used. To construct the space charge potentials, 1048576 macroparticles were tracked in 100 turns. After that, we fixed the space charge potentials (so-called "frozen model simulation") and tracked 160000 test particles. As well as the user operation, the second-harmonic RF cavities were used in this simulation. With reference to the longitudinal beam distribution (see top panel of Fig. 2), the initial

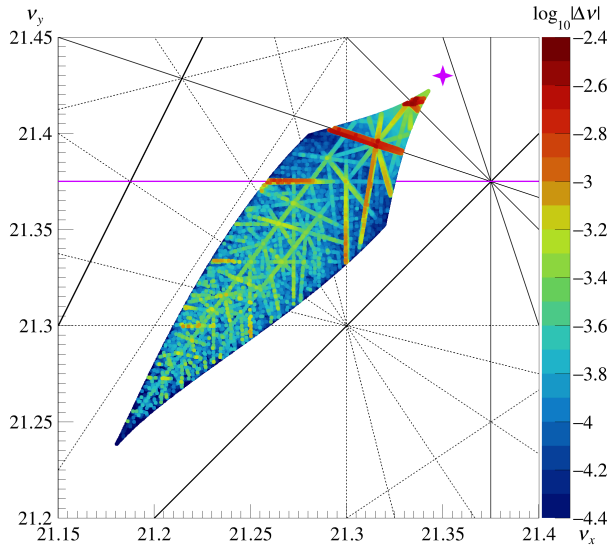

Figure 11: FMA with the present optics. The magenta line denotes the resonance $8\nu_y = 171$.

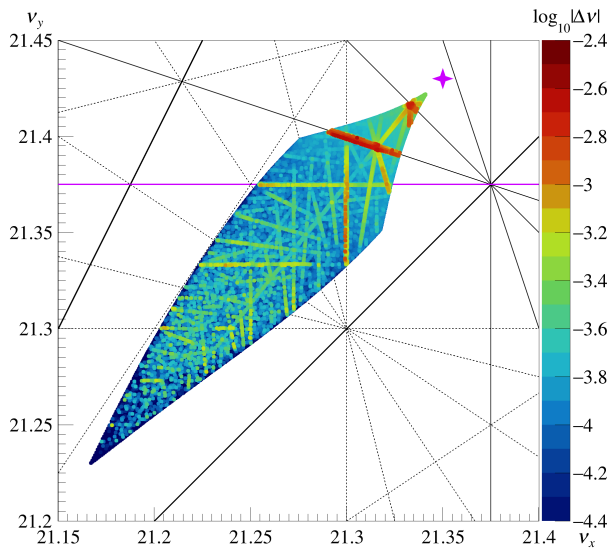

Figure 12: FMA with the new optics. The magenta line denotes the resonance $8\nu_y = 171$.

longitudinal positions of the test particles were set at the local minimum point $(z, \delta) \simeq (-22\,\mathrm{m}, 0)$. The test particles were almost fixed longitudinally. The peak-to-peak sizes of longitudinal oscillations were $\Delta z \sim 0.8$ mm and $\Delta\delta \sim 8 \times 10^{-8}$. The line density at that point was $\lambda \simeq 3.8 \times 10^{11}$ ppb/m. The oscillation period was approximately 300 turns, which corresponds to half of the synchrotron period. The tunes were calculated for first (ν_1) and second (ν_2) oscillations using NAFF [12] with the Hanning window. Defining the tune shift as $|\Delta\nu| \equiv \sqrt{(\nu_{x,2} - \nu_{x,1})^2 + (\nu_{y,2} - \nu_{y,1})^2}$, we used $\log_{10}|\Delta\nu|$ as the indicator of FMA. Figures 11 and 12 show the results of FMA with the present and new optics, respectively. In the present optics, the resonance $8\nu_y = 171$ can be seen as a red line, while in the new optics it is a yellow

ISBN: 978-3-95450-253-0 ISSN: 2673-5571 doi:10.18429/JACoW-HB2023-WEA2I2

line. These FMA results also indicate that the resonance $8\nu_y = 171$ is weakened in the new optics.

CONCLUSIONS AND OUTLOOK

In the J-PARC MR, the effect of space-charge-induced resonances is one of the constraints to increase the beam intensity. Since the supreperiodicity of the MR is only three, high-order structure resonances are inevitable. By conducting a survey of the lost particles in simulations, we found that the eighth-order space-charge-induced structure resonance $8\nu_y = 171$ is the primary cause of the beam loss when excluding magnet imperfections. This is because the resonance $8\nu_y = 171$ affects particles at beam halo. We noted that even after optimizing the working point, the resonance strength can be altered by rebalancing the phase advances. By changing the vertical phase advances in the arc section $\Delta\psi_{y,\mathrm{arc}}$ and maintaining the working point, we developed a new beam optics to suppress the resonance $8\nu_y = 171$ and reduce the beam loss. The superiority of the new optics was confirmed via analytical calculations of the resonance potential $U_{0,8,171}$, beam loss simulations, Poincaré map simulations, FMA simulations, and beam loss measurements.

Beam studies of the new optics were conducted before the long-term shutdown in JFY2022. Although some magnets did not have capacity for ramping up to 30 GeV with the new optics at that time, now all magnets can owing to the upgrade. The new optics should be applied as soon as the power supply adjustments are completed. The upgrade of magnet power supplies also made it possible to set the working point in $(\nu_x, \nu_y) = (22.*, 22.*)$ area. Since the resonances $\nu_x = 21$ and $\nu_y = 21$ are structure resonances, it is expected that $(\nu_x, \nu_y) = (22.*, 22.*)$ area has wider tunability. Even when exploring $(\nu_x, \nu_y) = (22.*, 22.*)$ area, the method of resonance identification and $\Delta\psi_{y,\mathrm{arc}}$ scan proposed in this paper will be utilized. These findings can be applied not only in the J-PARC MR but also other hadron synchrotrons. For example, they will be useful in designing and evaluating new synchrotrons.

REFERENCES

[1] T. Koseki *et al.*, "Beam commissioning and operation of the J-PARC main ring synchrotron", *Prog. Theor. Exp. Phys.*, vol. 2012, p. 02B004, 2012. doi:10.1093/ptep/pts071

[2] S. Igarashi *et al.*, "Accelerator design for 1.3-MW beam power operation of the J-PARC main ring", *Prog. Theor. Exp. Phys.*, vol. 2021, p. 033G01, 2021. doi:10.1093/ptep/ptab011

[3] T. Yasui, "J-PARC MR operation with the high repetition rate upgrade", in *Proc. IPAC'23*, Venice, Italy, May 2023, TUXG1, pp. 1294–1298. doi:10.18429/JACoW-IPAC2023-TUXG1

[4] T. Yasui and Y. Kurimoto, "Suppression of the eighth-order space-charge-induced resonance", *Phys. Rev. Accel. Beams*, vol. 25, p. 121001, 2022. doi:10.1103/PhysRevAccelBeams.25.121001

[5] K. Ohmi, S. Igarashi, H. Koiso, T. Koseki, and K. Oide, "Study of halo formation in J-PARC MR", in *Proc. PAC-2007*, Albuquerque, NM, USA, Jun. 2007, pp. 3318–3320. http://jacow.org/p07/PAPERS/THPAN040.PDF

[6] K. Ohmi, "Artificial noise in PIC codes and consequences on long term tracking", in *Proc. HB'14*, East-Lansing, MI, USA, Nov. 2014, pp. 259–266. https://jacow.org/HB2014/papers/weo2lr03.pdf

[7] S. Igarashi, "Recent progress of J-PARC MR beam commissioning and operation", in *Proc. HB'16*, Malmö, Sweden, Jul. 2016, pp. 21–26. doi:10.18429/JACoW-HB2016-MOAM6P60

[8] Y. Sato, "High power beam operation of the J-PARC RCS and MR", in *Proc. IPAC'18*, Vancouver, BC, Canada, May 2018, pp. 2938–2942. doi:10.18429/JACoW-IPAC2018-THYGBF1

[9] M. Bassetti and G. A. Erskine, "Closed expression for the electrical field of a two-dimensional Gaussian charge", Report No. CERN-ISR-TH/80-06, 1980. https://cds.cern.ch/record/122227

[10] S. Kheifets, "Potential of a three-dimensional Gaussian bunch", Technical Report PETRA Note No. 119, 1976. doi:10.3204/PUBDB-2017-01789

[11] K. Ohmi and K. G. Sonnad, "Beta function measurement and resonances induced by space charge force and lattice magnets", in *Proc. IPAC'16*, Busan, Korea, May 2016, pp. 641–643. doi:10.18429/JACoW-IPAC2016-MOPOR019

[12] J. Laskar, C. Froeschlé, and A. Celletti, "The measure of chaos by the numerical analysis of the fundamental frequencies. Application to the standard mapping", *Physica*, vol. 56D, p. 253, 1992. doi:10.1016/0167-2789(92)90028-L